# Title: The inner membrane protein YhdP modulates the rate of anterograde phospholipid flow in *Escherichia coli*

**Authors:** Jacqueline Grimm[1,†], Handuo Shi[2,†], Wei Wang[3], Angela M. Mitchell[1,4], Ned S. Wingreen[1,3], Kerwyn Casey Huang[2,5,6,*], Thomas J. Silhavy[1,*]

**Affiliations**

[1]Department of Molecular Biology, Princeton University, Princeton, NJ 08544, USA

[2]Department of Bioengineering, Stanford University School of Medicine, Stanford, CA 94305, USA

[3]Lewis-Sigler Institute for Integrative Genomics, Princeton University, Princeton, NJ 08544, USA

[4]Department of Biology, Texas A&M University, College Station, TX 77843

[5]Department of Microbiology & Immunology, Stanford University School of Medicine, Stanford, CA 94305, USA

[6]Chan Zuckerberg Biohub, San Francisco, CA 94158

[†]: These authors contributed equally.

*Corresponding authors: tsilhavy@princeton.edu and kchuang@stanford.edu

*Keywords:* MlaA, Gram-negative, cell envelope, AsmA, enterobacterial common antigen, cell mechanics, permeability barrier, cell death, single-cell microscopy, lipid homeostasis, lipid transport

## Abstract

The outer membrane (OM) of Gram-negative bacteria is a selective permeability barrier that allows uptake of nutrients while simultaneously protecting the cell from harmful compounds. The basic pathways and molecular machinery responsible for transporting lipopolysaccharides (LPS), lipoproteins, and β-barrel proteins to the OM have been identified, but very little is known about phospholipid (PL) transport. To identify genes capable of affecting PL transport, we screened for genetic interactions with *mlaA**, a mutant in which anterograde PL transport causes the inner membrane (IM) to shrink and eventually rupture; characterization of *mlaA**-mediated lysis suggested that PL transport can occur via a high-flux, diffusive flow mechanism. We found that YhdP, an IM protein involved in maintaining the OM permeability barrier, modulates the rate of PL transport during *mlaA**-mediated lysis. Deletion of *yhdP* from *mlaA** reduced the rate of IM transport to the OM by 50%, slowing shrinkage of the IM and delaying lysis. As a result, the weakened OM of Δ*ydhP* cells was further compromised and ruptured before the IM during *mlaA**-mediated death. These findings demonstrate the existence of a high-flux, diffusive pathway for PL flow in *Escherichia coli* that is modulated by YhdP.

## Significance Statement

The outer membrane (OM) of Gram-negative bacteria serves as a barrier that protects cells from harmful chemical compounds, including many antibiotics. Understanding how bacteria build this barrier is an important step in engineering strategies to circumvent it. A long-standing mystery in the field is how phospholipids (PLs) are transported from the inner membrane (IM) to the OM. We previously discovered that a mutation in the gene *mlaA* causes rapid flow of PLs to the OM, eventually resulting in IM rupture. Here, we found that deletion of the gene *yhdP* delayed cell death in the *mlaA* mutant by slowing flow of PLs to the OM. These findings reveal a high-flux, diffusive pathway for PL transport in Gram-negative bacteria modulated by YhdP.

## Introduction

The outer membrane (OM) of Gram-negative bacteria is an asymmetric bilayer composed of lipopolysaccharides (LPS) in the outer leaflet and PLs in the inner leaflet (1). Strong lateral interactions between LPS molecules in the outer leaflet result in a bilayer that is impermeable to both hydrophobic and large hydrophilic compounds (2). In addition to its role as a permeability barrier, β-barrel proteins and lipoproteins in the OM play key roles in a variety of other important processes, including motility, pathogenesis, and cell division (3). Because the periplasm lacks conventional sources of energy such as ATP, Gram-negative bacteria face a significant challenge in transporting and assembling OM components. To circumvent this challenge, cells utilize ATP hydrolysis in the inner membrane (IM) to transport LPS molecules across a protein bridge that spans the periplasm (4, 5). β-barrel proteins and lipoproteins also use ATP hydrolysis to cross the IM, but are escorted across the periplasm by soluble carriers (6, 7).

While relatively little is known about the transport of PLs to the OM, current understanding points to a mechanism that is highly distinct from the known OM transport pathways. Liposome fusion experiments in *Salmonella* Typhimurium demonstrated that unlike proteins and LPS, PL transport is bidirectional and indiscriminate (8). Rapid transfer from the OM to the IM was observed for all major and

minor species of *Salmonella* PLs and even for cholesteryl oleate, which is not a normal component of bacterial membranes (8). One explanation consistent with these findings is that PLs can be transported by diffusional flow. Diffusive PL transport could occur at zones of hemifusion that form spontaneously. Diffusion could also require protein facilitators, for instance to encourage formation of hemifusions or to form protein channels through which PLs flow.

Although the bacterial PL transport pathway is currently unknown, the mechanisms by which cells maintain asymmetry in the OM are much better understood. When the integrity of the outer leaflet is disrupted, PLs from the inner leaflet migrate to fill gaps in the LPS, creating zones that are newly permeable to toxic hydrophobic compounds. The cell remedies this problem using the Mla (**M**aintenance of **l**ipid **a**symmetry) pathway, which removes mislocalized PLs from the outer leaflet and shuttles them to the IM (9). MlaA is a donut-shaped lipoprotein that sits in the outer membrane, removes PLs from the outer leaflet, and delivers them to the soluble carrier, MlaC. MlaC then transports them across the periplasm to the MlaFEDB complex, an ABC transport system that unloads MlaC and returns PLs to the IM.

In *E. coli*, a dominant negative mutation in *mlaA*, called *mlaA**, reverses the protein's normal function (10). Instead of removing surface-exposed PLs, MlaA* allows properly

localized PLs to flow through its pore into the outer leaflet (10, 11). Accumulation of PLs in the outer leaflet triggers a cell death pathway that results in lysis during stationary phase (10). First, the presence of PLs in the outer leaflet activates the OM phospholipase PldA, which cleaves surface-exposed PLs, generating breakdown products that signal to increase production of LPS (12). Hyper-production of LPS destabilizes the OM, resulting in loss of OM material through blebbing. PLs then flow from the IM to the OM to replace the lost material. In stationary phase, cells can no longer synthesize new PLs to replace those lost from the IM. As a result, PL flow causes the IM to shrink and ultimately rupture.

We hypothesized that changing the rate of PL flow from the IM to the OM would affect the rate of lysis in *mlaA** cells, since PL flow to the OM is what eventually causes the IM to rupture. Hence, we should be able to identify genes that affect PL transport through genetic interactions with *mlaA**. Our screen identified *yhdP*, a gene already known to play a role in maintaining the barrier function of the OM (13). Deletion of *yhdP* slowed lysis, but did not restore wild-type LPS levels, indicating that it affects a step in the pathway after LPS levels have already increased. Single-cell microscopy showed that the IM of *mlaA** Δ*yhdP* cells shrank more slowly, implying slower anterograde flow. In *mlaA** cells, PL flow ultimately leads to IM rupture but also compensates for loss of OM material while cells are actively growing. By contrast, without YhdP, the OM ruptured

before the IM, suggesting that these cells cannot efficiently compensate for OM loss through anterograde flow.

112 # Results

113 ## *mlaA** causes high-flux, passive phospholipid flow

114 It was previously shown that PL flow in *mlaA** cells is not affected by membrane
115 depolarization or ATP synthase mutations, indicating that flow occurs via a passive
116 mechanism (11). To further characterize this pathway, we quantified the rate of
117 anterograde flow. We induced the cell division inhibitor SulA (14) and then transitioned
118 exponentially growing cells onto agarose pads containing spent medium to cause the
119 *mlaA** death phenotype. The SulA-induced cells became filamentous, and hence we
120 could quantify the IM shrinkage from one of the poles prior to cell death (Figure 1A,
121 white arrows) more easily than in non-filamentous cells. Since IM shrinkage in *mlaA**
122 cells is the result of PL transport to the OM (10), we measured the rate of shrinkage as a
123 proxy for the PL transport rate.

124

125 The IM shrunk by ~20% in approximately 20 min (Figure 1B,C), corresponding to a PL
126 flow rate of 1.2 ± 0.4% of the cell length per min. That a substantial fraction of the IM
127 can be transported quickly even under the energetic limitations that occur upon entry
128 into stationary phase provides further evidence that PL flow can occur via a diffusive
129 mechanism. It also shows that the diffusive pathway is high-flux, permitting transport
130 of a large proportion of the IM within a short period of time.

131

132 **Genetic interactions with *mlaA** depend on the length of time in spent medium**

133 To identify genetic interactions with *mlaA**, we constructed transposon insertion
134 libraries in *mlaA** and Δ*mlaA* cells. We grew the libraries to late exponential phase and
135 incubated them in spent medium overnight to induce lysis. We repeated this process
136 three times successively, inferring that the survival of any mutant that suppressed
137 *mlaA**-mediated cell death would be amplified by the repeated incubations.

138

139 As expected, by far the most abundant hit was *mlaA*, since null mutations in *mlaA**
140 prevent production of the mutant protein, completely suppressing cell death (10). The
141 next most abundant hit was *pldA*, again expected as without PldA, there is no signal to
142 increase production of LPS (10). After three rounds of incubation, insertions in *mlaA*
143 and *pldA* accounted for 96.3% of all reads. Among the other hits (Table 1), several were
144 known to affect LPS levels, corresponding to the results of a previous low-throughput
145 screen, which also identified several suppressor mutations that lowered LPS levels (10).
146 Since overproduction of LPS is a critical step in the cell-death pathway, mutations that
147 restore wild-type LPS levels are expected to suppress lysis independent of any potential
148 impact on PL transport (10). We therefore sought to find a genetic disruption that
149 suppressed *mlaA** without lowering LPS levels.

150

Since the most potent suppressors of *mlaA** block the earliest steps of the pathway, we hypothesized that slowing PL flow, the final step in the pathway, would only slow lysis. Hence, we carried out a similar experiment in which cells were only incubated for two hours in spent medium rather than overnight, to identify partial suppressors of *mlaA** (Figure 1D). Now, the most abundant hit in the *mlaA** library was *yhdP*, a large (1266 amino acid) IM protein. Interestingly, another member of its protein family, *asmA*, was identified as a suppressor in the previous screen (Table 1). YhdP has been shown to enhance OM permeability barrier function during stationary phase, but its mechanism is currently unknown (13). Deletion of *yhdP* causes sensitivity to SDS/EDTA and vancomycin regardless of growth phase, indicating that it plays a role in maintaining OM integrity (15). To confirm that disruption of *yhdP* inhibits lysis, we grew *mlaA** Δ*yhdP* cells to late exponential phase, resuspended them in spent medium, and measured OD over time; deletion of *yhdP* slowed the rate of lysis of *mlaA** cells (Figure 1E).

**Deletion of *yhdP* slows *mlaA** lysis without lowering LPS levels**

Since modulating PL flow would affect a step in the cell death pathway after LPS levels have already increased, we expected that inhibiting PL flow would slow *mlaA** lysis without restoring wild-type LPS levels. To test the effects of *yhdP* deletion on *mlaA** cells, we measured LPS levels by immunoblotting (Methods). Deletion of *yhdP* had no

effect on LPS levels either alone or in combination with *mlaA**, suggesting that it affects a later step in the pathway (Figure 1F). In addition, this finding suggests that *yhdP* does not slow lysis by affecting LPS transport, as it has been shown that slowing transport of LPS also reduces LPS levels (13).

**Deletion of *yhdP* slows shrinking of the IM**

In *mlaA** cells, shrinking of the IM away from the cell pole is thought to reflect anterograde PL flow to the OM (10). We therefore expected that a mutation that slows PL flow would also slow IM shrinking. To determine whether *yhdP* deletion affects PL flow, we imaged *mlaA** or *mlaA** Δ*yhdP* cells during incubation in a microfluidic flow cell. Cells were first kept in LB until they reached steady-state growth, and then rapidly switched into spent medium. With continuous flow of spent medium, all *mlaA** cells died within 20-30 min (10). Deletion of *yhdP* delayed cell death (Figure 2A), consistent with the dynamics in bulk culture (Figure 1E).

For both strains, the cytoplasm started to shrink immediately upon the transition to spent medium. The cytoplasm of *mlaA** cells shrank by an average of ~0.7 μm (20%, Figure 2B,C) over ~20 min (Figure 2A) and appeared to increase in density, followed by a "popping" expansion and then gradual loss of phase contrast (Figure 2B) that we previously characterized as typical of *mlaA**-mediated death (10). *mlaA** Δ*yhdP* cells

191 displayed a qualitatively similar death trajectory (Figure 2B). The average time to lysis
192 was longer (29 min, Figure 2A) and yet less shrinkage occurred (0.5 μm, 15%, Figure
193 2B,C) before popping than in *mlaA** cells. In both strains, the expansion at cell death
194 roughly restored cell length to the pre-shrinkage size (Figure 2C,D), suggesting that the
195 cell envelope returned to a relaxed state after the expansion. Shrinkage rate prior to
196 popping was also slowed down in *mlaA** Δ*yhdP* cells by 50% (Figure 2E). Taken
197 together, these data indicate that YhdP plays an important role in PL transport during
198 *mlaA**-mediated lysis.
199
200 **The effect of YhdP on lysis is cyclic ECA-independent**
201 It was previously shown that the OM permeability phenotypes of Δ*yhdP* cells can be
202 suppressed by preventing synthesis of cyclic enterobacterial common antigen (ECA),
203 indicating that YhdP regulates cyclic ECA (15). To test whether the effect of *yhdP*
204 deletion on *mlaA**-mediated lysis also depends on cyclic ECA, we constructed strains
205 lacking *wzzE*. WzzE is the ECA chain length regulator, and in its absence cyclic ECA is
206 not synthesized. If the effect of *yhdP* deletion on lysis rate also depends on cyclic ECA,
207 we would expect that deleting *wzzE* in *mlaA** Δ*yhdP* cells would reverse the effect of
208 *yhdP* deletion, resulting in dynamics upon transition to spent medium similar to that of
209 *mlaA** alone.
210

211 To quantify the effect of cyclic ECA in *mlaA** cells, we imaged *mlaA** Δ*yhdP* Δ*wzzE* cells
212 in a microfluidic device during the transition to spent medium. Deletion of *wzzE* did not
213 restore *mlaA**-like death dynamics (Figure 3A), nor did it change the shrinkage rate of
214 the *mlaA** Δ*yhdP* strain (Figure 3B). Deletion of *wzzE* did not affect the death (Figure 3A)
215 or shrinkage (Figure 3B) of *mlaA** cells, indicating that the effect of YhdP on PL
216 transport during *mlaA**-mediated lysis does not require cyclic ECA.
217
218 **Deletion of *yhdP* weakens the OM chemically and mechanically**
219 Another explanation for how deletion of *yhdP* could slow lysis is by preventing loss of
220 OM material. To test whether deleting *yhdP* improves OM integrity in *mlaA** cells, we
221 assayed OM permeability by plating on vancomycin or SDS/EDTA. It was previously
222 shown that cells lacking *yhdP* are vancomycin-sensitive (15). However, by plating on a
223 low concentration of vancomycin such that wild-type, *mlaA**, and Δ*yhdP* cells all grew
224 to the same dilution as on LB without drug, we observed that *mlaA** Δ*yhdP* cells had a
225 synthetic OM permeability defect (Figure 4A). On SDS/EDTA, *mlaA** and Δ*yhdP* were
226 both sensitive; combining the two mutations did not relieve the defect (Figure 4A).
227 These results demonstrate that deletion of *yhdP* does not slow lysis by enhancing OM
228 integrity.
229

230 Since deleting *yhdP* increased OM permeability in *mlaA** cells, we wondered whether
231 inhibition of anterograde flow might be due to destabilization of the OM. To further
232 characterize the effect of YhdP on the OM, we investigated its impact on OM
233 mechanical strength. In a previous study, we showed that the mechanical stiffness of
234 the *E. coli* OM is greater than or comparable to that of the cell wall, and that genetic or
235 chemical perturbations to the OM can reduce the overall stiffness of cells (16). To
236 determine if YhdP plays a role in determining OM stiffness, we utilized an assay in
237 which exponentially growing cells are first exposed to a large, hyperosmotic shock with
238 3 M sorbitol, and then treated with EDTA. We used a microfluidic flow cell to precisely
239 control the timing of treatments and track single cells throughout (Methods). Upon the
240 shock, wild-type cells experienced a large decrease in the length of the fluorescently
241 labeled cell wall (Figure 4B), as expected since turgor pressure was relieved and hence
242 the cell wall-OM envelope complex was no longer under stress. EDTA treatment, which
243 disrupts the OM by rapidly inducing loss of LPS molecules (17, 18), led to a further
244 decrease in cell length (Figure 4B), signifying that the stiff OM was holding the cell wall
245 out beyond its rest length before its removal. Application of this assay to Δ*yhdP* cells
246 showed greater contraction of the cell wall after the osmotic shock (Figure 4B,C) and
247 after EDTA treatment (Figure 4B,D), indicating that the overall stiffness of Δ*yhdP* cells
248 was lower than that of wildtype.
249

To further test whether deletion of *yhdP* weakened cells mechanically, we quantified the yield of viable cells after breaking down the cell wall using beta-lactam antibiotics to form wall-less spheroplasts with intact IM and OM (Methods). We previously showed that spheroplast yield is strongly correlated with the stiffness of the OM across chemical and genetic perturbations (16). In this assay, spheroplasts were generated overnight in the presence of cefsulodin, and then were washed and plated on fresh medium without antibiotics after the cell wall was removed. Survival in the absence of a cell wall relies on having a stiff outer membrane to bear the stress of turgor. We observed that *mlaA** and *yhdP* deletion each caused a dramatic (>1000-fold) decrease in spheroplast viability in comparison with wildtype (Figure 4E). The *mlaA** Δ*yhdP* double mutant exhibited a further decrease in spheroplast viability, highlighting the importance of YhdP in determining OM stiffness. However, deletion of *wzzE* partially suppressed the decrease in spheroplast viability due to Δ*yhdP* (Figure 4E), demonstrating that the effect of YhdP on OM mechanical strength is cyclic ECA-dependent.

Taken together, these results suggest that deleting *yhdP* does not slow lysis by preventing loss of OM material. Deletion of *yhdP* severely disrupts OM integrity, which is more likely to promote loss of OM material than to prevent it. Furthermore, *yhdP* deletion still slows lysis even when its effect on the mechanical strength of the OM is

suppressed (Figure 3A,B, Figure S1), indicating that *yhdP*'s effect on lysis is not a result of its effect on OM mechanics.

**Impairment of phospholipid flow leads to OM rupture**

We observed that the IM of *mlaA** Δ*yhdP* cells shrank more slowly and less relative to *mlaA** (Figure 2B-E). We would expect that a mutation that decreases PL flow would cause the IM to shrink more slowly. To explain why the IM shrank less before lysis, we wondered whether, in these cells, lysis occurs for a reason other than IM rupture. In *mlaA**, anterograde flow leads to rupture of the IM, followed shortly by OM rupture (10). We surmised that impairing PL flow in *mlaA** cells would increase the stress on the OM, potentially causing the OM to rupture before the IM.

To test this hypothesis, we constructed *mlaA** and *mlaA** Δ*yhdP* strains expressing both a cytoplasmic and a periplasmic fluorescent protein. When the *mlaA** strain was shifted into spent medium, shrinkage of the IM led to a large periplasmic space with high mCherry signal (Figure 5A, white arrow). The mCherry signal remained intact throughout shrinkage, and when the cells popped and lysed, periplasmic mCherry and cytoplasmic GFP signals were lost simultaneously in every cell (Figure 5A,B), presumably because rupture of the IM also led to rapid OM rupture (10). By contrast, in *mlaA** Δ*yhdP* cells, the extent of IM shrinkage was much smaller (Figure 2C), and the

289 periplasmic mCherry signal remained largely uniform around cell periphery rather
290 than intensified at a cell pole(s) (Figure 5C). During the transition to spent medium, the
291 mCherry signal was lost tens of minutes before popping (Figure 5C,D), while the
292 cytoplasmic YFP signal remained intact until popping occurred (Figure 5C). Taken
293 together, these data indicate that disruption of anterograde flow caused by *yhdP*
294 deletion in *mlaA** Δ*yhdP* cells leads to rupture of the OM before the IM (Figure 5E).

295 **Discussion**

296 The existence of fusion junctions facilitating PL flow between the IM and OM has been
297 a matter of controversy for some time. In the 1960s, electron microscopy showed sites of
298 contact between the two membranes, but improved microscopy methods called into
299 question the existence of these "Bayer's junctions" (19, 20). While it may be the case that
300 the junctions observed in those early images were indeed artifacts, several lines of
301 evidence now suggest that intermembrane PL transport can occur via diffusion.

302

303 Previous studies showed that PL transport is bidirectional and can involve even non-
304 native lipids (8, 21). In the *mlaA** mutant, PL flow does not require either ATP or proton
305 motive force (11). In addition, in this mutant approximately 20% of the IM is lost by
306 transport even under the nutrient limitations that trigger entry into stationary phase.
307 These data are strong evidence that PL flow in *mlaA** cells is passive, and occurs
308 through a high-flux pathway. It remains to be seen whether this pathway functions in
309 normal PL transport or is active only in certain conditions.

310

311 In this study, we provide evidence that YhdP is involved in modulating the high-flux
312 PL transport pathway. Time-lapse imaging showed that deleting *yhdP* slowed shrinkage
313 of the IM in *mlaA** cells (Figure 2), implying that PLs flowed more slowly from the IM to
314 the OM. In *mlaA**, loss of lipids from the IM ultimately causes it to rupture (10). As a

result, slowing PL flow delays cell death. However, since PL flow also compensates for loss of OM material, slowing flow from the IM comes at the cost of OM integrity. Thus, while lysis takes longer in *mlaA** Δ*yhdP* cells, when it does occur, the OM rather than the IM ruptures first (Figure 5D).

Cells survive without *yhdP*, suggesting that YhdP functions specifically in high-flux PL transport. If it does play a role in normal PL transport, then there must be multiple, redundant pathways. How YhdP modulates PL transport is still unknown, but an intriguing possibility is suggested by its protein family. YhdP belongs to a family of six "AsmA-like" proteins (AsmA, TamB, YdbH, YicH, YhjG, and YhdP). Two members of this family, AsmA and TamB, are predicted to share homology with the eukaryotic PL transporter, Vps13 (22). Vps13 forms a hydrophobic channel through which PLs are transported between membranes (23, 24). The structure of TamB also includes a channel with a highly hydrophobic interior (25). Interestingly, it has been suggested that due to its ability to accommodate many lipids at once, Vps13 functions specifically in high-flux PL transport (26).

While our study does not determine YhdP's molecular mechanism, it does rule out certain possibilities. Deleting *yhdP* does not lower LPS levels (Figure 1F), hence it must affect a step in the *mlaA** death pathway after LPS levels have already increased.

335 Moreover, the effect of *ydhP* deletion on *mlaA** lysis cannot be explained by slowed
336 transport of LPS to the OM, as it has previously been shown that slowing LPS transport
337 also decreases LPS levels (12). It is also unlikely that deleting *yhdP* slowed lysis (Figure
338 2A,B) by preventing loss of OM material, as *yhdP* deletion has a severe negative impact
339 on OM integrity (Figure 4). Of the remaining options, a direct role in transport is
340 certainly the simplest. YhdP is a large (1266 amino acid) IM protein with one clear N-
341 terminal and possibly a second, C-terminal transmembrane domain. Given the size of
342 its periplasmic domain, it is plausible that YhdP can span the periplasm, but further
343 structural and biochemical studies are needed to determine its precise role in
344 anterograde PL transport. Regardless, our data provide new insight into the process of
345 PL flow and cell lysis caused by the dominant negative *mlaA** allele, and shed light on
346 the multiple roles played by YhdP in the maintanence of OM integrity. The fact that
347 YdhP changes both OM stiffness and permeability suggests an intriguing link between
348 these two properties. Our discovery of a mutant capable of slowing PL transport should
349 provide a useful foothold in the investigation of this poorly understood pathway.

# Methods

## Bacterial strains

The strains used in this study are listed in Table S1. Strains were constructed by generalized P1 transduction with all deletions originating from the Keio collection (27, 28). Kanamycin resistance cassettes were removed using the Flp recombinase system, as previously described (29). Overnight cultures were grown at 37 °C in lysogeny broth (LB) medium supplemented with 10 mM $MgSO_4$ to prevent *mlaA** lysis and diluted into unsupplemented LB for subsequent experiments. When necessary, media were supplemented with 25 μg/mL kanamycin or 25 μg/mL tetracycline.

## TraDIS sample preparation

Transposon mutant libraries were constructed using the EZ-Tn5<KAN-2>TnP Transposome Kit (Epicentre) according to the manufacturer's instructions. When preparing electrocompetent cells, overnight cultures were grown in LB supplemented with 5 mM $MgSO_4$ to prevent lysis of *mlaA** and then subcultured in 2xYT medium. Following electroporation, cells were plated on LB+25 μg/mL kanamycin plates supplemented with 5 mM $MgSO_4$. Approximately 300,000 and 150,000 colonies were pooled to construct the *mlaA** and Δ*mlaA* libraries, respectively. Genomic DNA was extracted from samples of $2\times10^9$ cells after lysis using the DNeasy Blood and Tissue Kit

(Qiagen) according to the manufacturer's instructions. Libraries were prepared according to the TraDIS method (30) and sequenced on Illumina HiSeq 2500 Rapid flowcells as single-end, 75-nucleotide reads.

**TraDIS data analysis**

Sequencing reads were mapped to the *E. coli* K12 genome using BWA v. 1.2.3. Mapped reads were quantified using htseq-count v. 0.6.0. The Integrative Genomics Viewer was used to visualize the mapped reads.

**Lysis curves**

To generate spent medium, wild-type (MC4100) cultures were grown for 24 h in LB at 37 °C, cells were pelleted, and the supernatant was filter-sterilized using a 0.2-μm filter. All experiments were conducted using wild-type spent medium. To assay the rate of lysis, cultures were grown until $OD_{600}$~0.8, pelleted, and resuspended in spent medium. Cultures were then incubated at 37 °C and $OD_{600}$ was measured at 15-min intervals.

**Immunoblot analyses**

The equivalent of 1 mL of culture at $OD_{600}$~1 was taken from overnight cultures, pelleted, and resuspended in LDS sample buffer (Invitrogen). Samples were boiled for 10 min and allowed to cool. Samples were loaded on 4-12% SDS/polyacrylamide gel

390 electrophoresis (PAGE) gels and run at 100 V. LPS was then transferred to nitrocellulose
391 membranes and blocked in 5% non-fat dried milk for 1 h at room temperature.
392 Membranes were then incubated overnight at 4 °C with anti-LPS antibody (1:400,000;
393 Hycult Biotech) in milk. Membranes were washed and incubated with secondary
394 antibody for 1 h at room temperature (1:20,000; Goat Anti-Mouse IgG (H+L)-HRP
395 Conjugate; Bio-Rad).
396
397 **Efficiency of plating assay**
398 Cultures were grown overnight in LB + 10 mM $MgSO_4$, standardized by OD, and
399 serially diluted. Dilutions were then transferred to plates using a 96-well-plate replica
400 plater and incubated overnight at 37 °C.
401
402 **Single-cell imaging**
403 Cells were imaged on a Nikon Eclipse Ti-E inverted fluorescence microscope with a
404 100X (NA 1.40) oil-immersion objective (Nikon Instruments). Images were collected on
405 a DU885 electron-multiplying charged couple device camera (Andor Technology) or a
406 Neo sCMOS camera (Andor Technology) using μManager version 1.4
407 (http://www.micro-manager.org) (31). Cells were maintained at 37 °C during imaging
408 with an active-control environmental chamber (HaisonTech).
409

For experiments conducted on agarose pads, 1 μL of cells was spotted onto a pad of 1% agarose in fresh LB or spent medium. For transition experiments, exponentially growing cells were washed three times in spent medium before spotting. Flow-cell experiments were performed in ONIX B04A microfluidic chips (CellASIC) and medium was exchanged using the ONIX microfluidic platform (CellASIC).

**Imaging in microfluidic devices**

Overnight cultures were diluted 100-fold into 1 mL of fresh LB and incubated for 2 h with shaking at 37 °C. B04A plates were loaded with medium and pre-warmed to 37 °C. Cells were loaded into the plate, which was incubated at 37 °C, without shaking for 30 min before imaging. As necessary, the cell envelope was stained with wheat germ agglutinin-AlexaFluor488 (WGA-AF488, Life Technologies), which was added to the loading well to a final concentration of 10 μg/mL prior to loading cells into the imaging chamber. The osmolarity of the growth medium was modulated with sorbitol (Sigma).

During plasmolysis/lysis experiments to quantify the effect of *yhdP* deletion on cell stiffness, cells were allowed to grow for 5 min in medium in the imaging chamber before being plasmolyzed with LB + 3 M sorbitol and exposed to LB + 3 M sorbitol + 10 mM EDTA 5 min later.

430 **Image analysis**

431 Time-lapse images were first segmented with the software *DeepCell* (32), and the
432 resulting segmented images were analyzed using *Morphometrics* (33) to obtain cell
433 contours at sub-pixel resolution. Static images were directly segmented using
434 *Morphometrics* (33). Cell width and length were calculated using the MicrobeTracker
435 meshing algorithm (34).

436

437 **Quantification of spheroplast viability and growth**

438 Overnight cultures of the appropriate strains were diluted 1:100 into LFLB (LB
439 supplemented with 3.6% sucrose and 10 mM $MgSO_4$). Cultures were incubated at 37 °C
440 for 1 h, normalized to $OD_{600}$ ~ 0.08, at which point cefsulodin was added to a final
441 concentration of 60 μg/mL. Cells were further incubated for 12 h with shaking at 30 °C.
442 Ten microliters of serial ten-fold dilutions were plated on LFLB plates. Plates were
443 incubated at 30 °C for 24 h, and colony-forming units were counted manually.

## Acknowledgements

The authors thank the Huang and Silhavy labs for helpful suggestions and the Genomics Core Facility of Princeton University for next-generation sequencing experiments. This research was supported by the National Institute of General Medical Sciences of the National Institutes of Health under grants 5R35GM118024 (to T.J.S.) and T32-GM007388 (to J.G.). The authors acknowledge partial support from NIH Grant R01 GM082938 (N.S.W.) and support from a James McDonnell Postdoctoral Fellowship (to H.S.). K.C.H. is a Chan Zuckerberg Biohub Investigator.

## Figure Legends

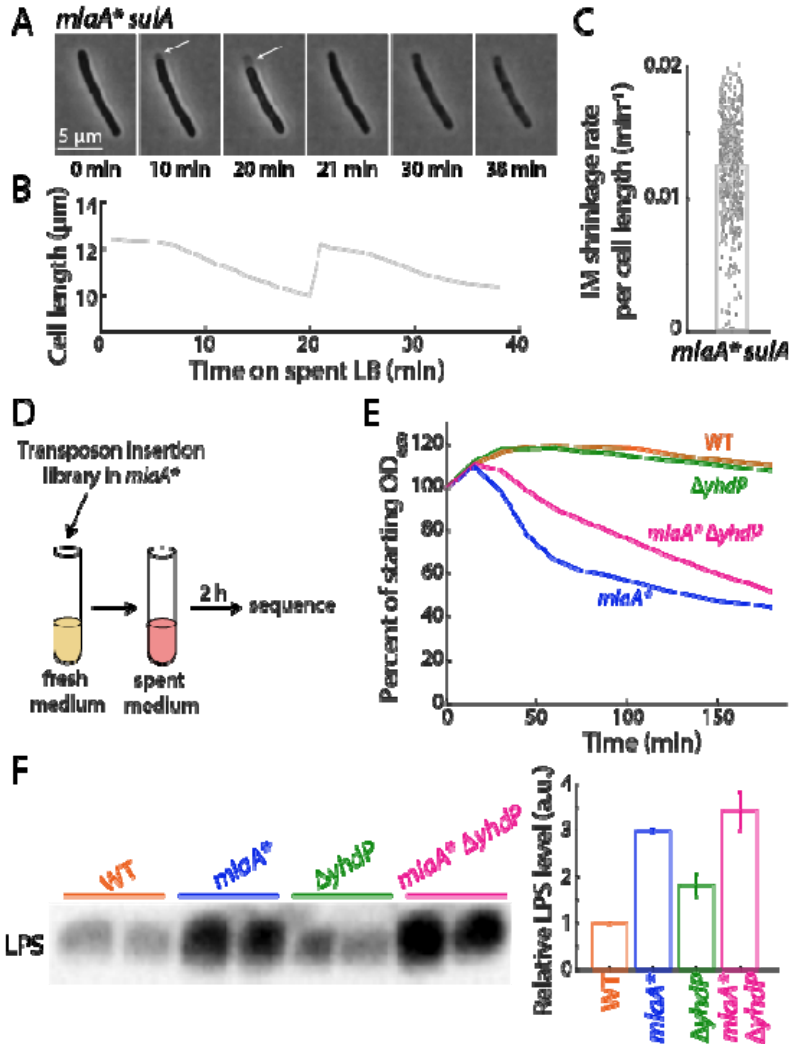


**Figure 1: Deletion of *yhdP* slows the rate of *mlaA** lysis.**

A) Exponentially growing *mlaA* sulA* cells were transitioned onto an agarose pad containing spent medium. In a typical cell, the IM shrank away from the cell wall (white arrows) before the cell eventually popped (*t*=21 min) and died.

B) Cell length of the cell in (A) initially decreased, then rapidly snapped back to approximately the initial size at the time of transition to spent medium, and finally decreased due to leakage.

C) During the initial 20 min in spent medium, the IM length shrank ~1% per minute. Each dot represents a single cell (total $n$ = 677 cells), and the bar represents mean ± standard deviation (S.D.).

D) Schematic of TraDIS selection. Libraries were grown into late exponential phase and transitioned to spent medium for 2 hours to induce lysis. The resulting library was subsequently sequenced for enrichment of mutants.

E) Cultures were grown to late exponential phase ($OD_{600}$ ~0.8), spun down, and resuspended in spent medium to induce lysis. $OD_{600}$ was measured to determine rate of lysis. Deletion of *yhdP* slowed down *mlaA**-mediated lysis. Data points are mean ± S.D. with $n$ = 3 replicates.

F) Overnight cultures were normalized by $OD_{600}$ and assayed for LPS abundance by immunoblotting. Left: immunoblotting gel image. Right: quantification of LPS abundances. Data points are mean ± S.D. with $n$ = 2 biological replicates. Deletion of *yhdP* did not affect LPS levels either alone or in combination with *mlaA**.

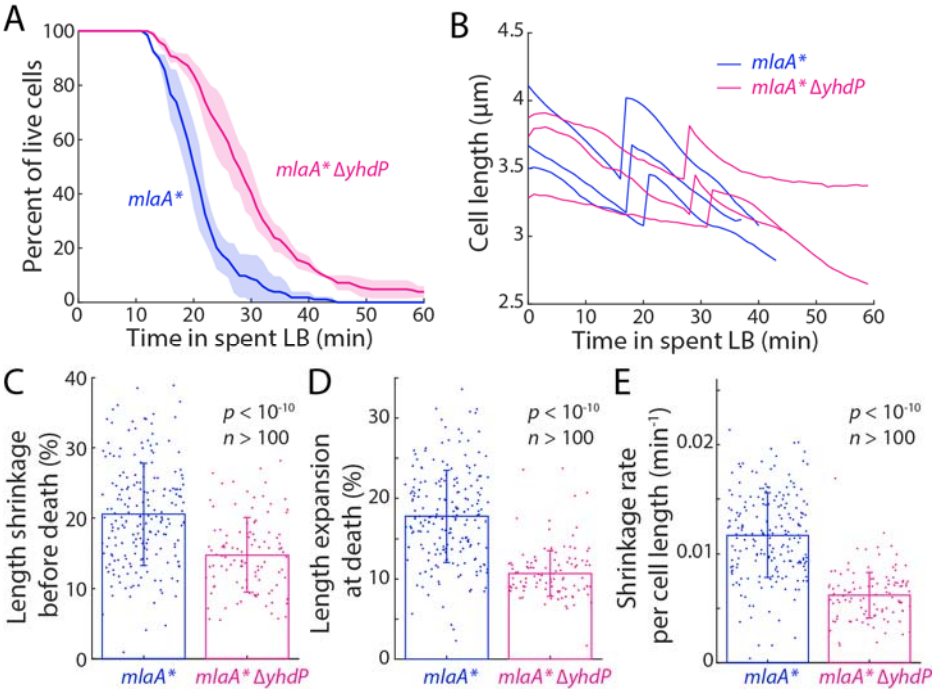


**Figure 2: Deletion of *yhdP* slows shrinking of the IM during transition to spent medium.**

A) *mlaA** and *mlaA** Δ*yhdP* cells were separately incubated in a microfluidic flow cell and transitioned from fresh LB to spent medium to induce cell death. Consistent with bulk measurements, deletion of *yhdP* slowed down cell death. Data points are mean ± S.D. with $n = 3$ replicates of at least 50 cells in each experiment.

B) Representative single-cell traces after switching to spent medium.

C) Deletion of *yhdP* reduced total shrinkage in *mlaA** cells by ~50% ($p < 10^{-10}$, $n > 100$ cells, two-tailed Student's *t*-test).

D) During the "popping" immediately preceding lysis, *mlaA** and *mlaA** Δ*yhdP* cells returned to approximately their initial length prior to the transition to spent medium (compare length expansion to the shrinkage in (C); *mlaA** cells exhibited

489 more expansion than *mlaA** Δ*yhdP* cells, $p < 10^{-10}$, $n > 100$ cells, two-tailed

490 Student's *t*-test).

491 E) Deletion of *yhdP* slowed down the shrinkage rate of *mlaA** cells ($p < 10^{-10}$, $n > 100$

492 cells, two-tailed Student's *t*-test).

493 In (C-E), each dot represents a single cell, and the bar plots represent mean ± S.D.

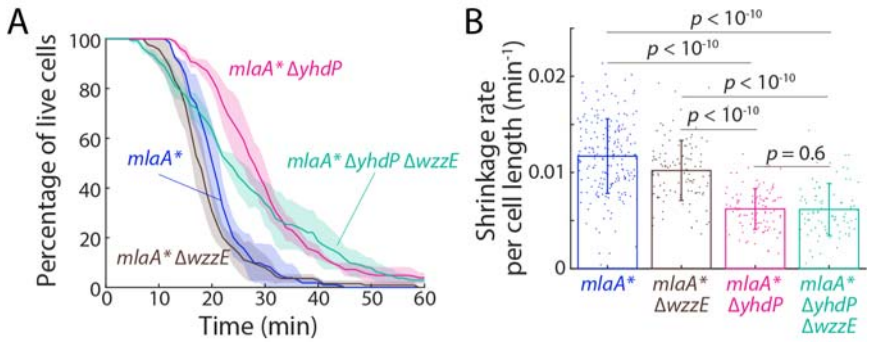


**Figure 3: Cyclic ECA is not responsible for suppression of death by Δ*yhdP*.**

A) Cells were incubated in a microfluidic flow cell and transitioned from fresh LB to spent medium to induce cell death. Deletion of the ECA biosynthesis gene *wzzE* did not restore *mlaA**-like lysis dynamics to *mlaA** Δ*yhdP*. *mlaA** Δ*yhdP* Δ*wzzE* cells exhibited distinct and slower death dynamics compared to *mlaA** cells, while deletion of *wzzE* from *mlaA** slightly accelerated cell death. Data points are mean ± S.D. with $n = 3$ replicates.

B) Deletion of *wzzE* did not alter the shrinkage rate of *mlaA** Δ*yhdP* cells ($n > 100$ cells) and only slightly reduced the rate in *mlaA** cells, indicating that the effect of YhdP on lysis is cyclic ECA-independent. Each dot represents a single cell ($n >$ 100 cells for each strain), and the bar plots represent mean ± S.D. *p*-values are from two-tailed Student's *t*-tests.

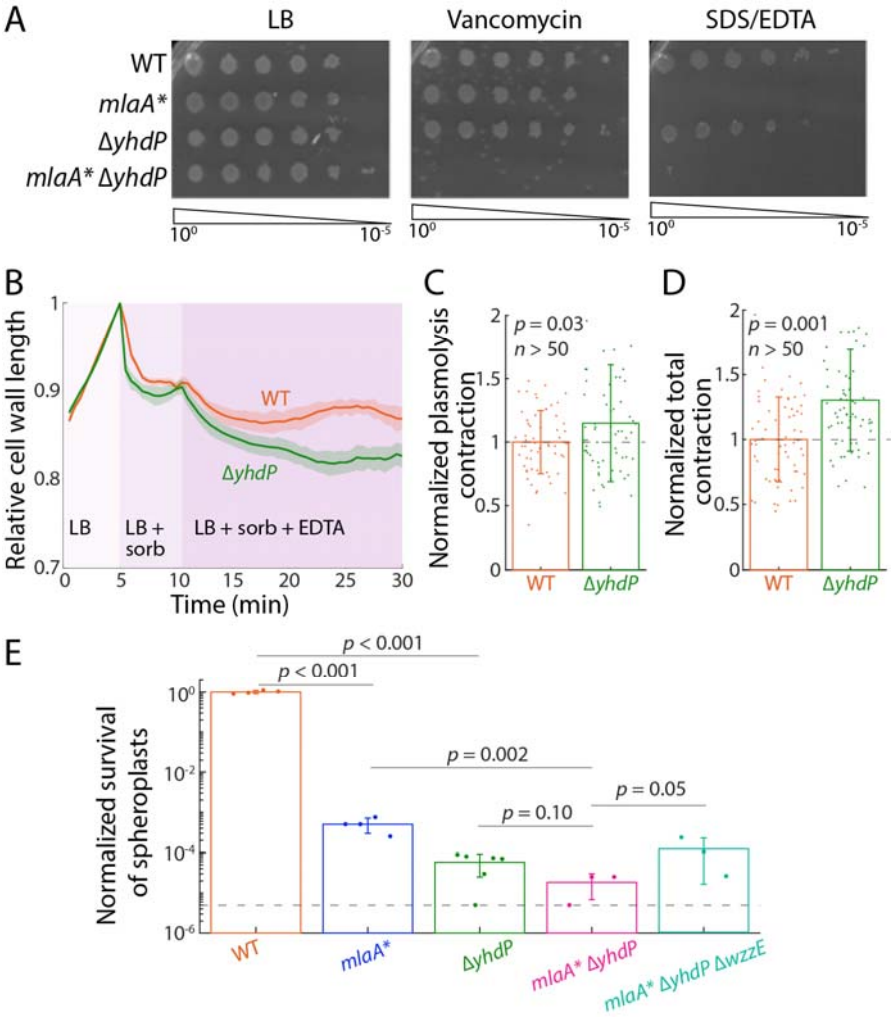


507

508 **Figure 4: Deletion of *yhdP* chemically and mechanically disrupts the OM.**

509 A) Overnight cultures were normalized by OD, serially diluted, and plated on LB,
510 LB + 20 μg/mL vancomycin, and LB + 0.5% SDS/0.5 mM EDTA. *mlaA** and Δ*yhdP*
511 have a synthetic permeability defect with vancomycin, and neither *mlaA** nor
512 *mlaA** Δ*yhdP* cells grew with SDS/EDTA.

513 B) Exponentially growing cells were loaded into a microfluidic device and allowed
514 to grow in LB before being exposed to a large hyperosmotic shock with 3 M
515 sorbitol, then treated with EDTA in the precence of sorbitol. The length of the

fluorescently labeled cell wall was tracked. Sorbitol treatment relieved turgor pressure and reduced cell-wall length. EDTA treatment disrupted the OM and led to a further decrease in cell length. In both conditions, Δ*yhdP* cells shrank more compared to wild-type cells.

C,D) Length contraction upon sorbitol (C) and EDTA (D) treatment for cells in (B). In both conditions, Δ*yhdP* cells shrank more than wildtype, indicating a mechanically weakened OM. Individual dots are data from single cells ($n$>50 for each strain), and bar plots represent mean ± S.D. $p$ values are from a two-tailed Student's $t$-test.

E) Spheroplasts were generated overnight in the presence of cefsulodin, and then washed and plated on fresh media. Both *mlaA** and Δ*yhdP* exhibited a mechanically weakened OM and reduced spheroplast survival rates. Deletion of *wzzE* partially rescued the mechanical defect in *mlaA** Δ*yhdP* cells. Dots represent biological replicates ($n$>3 replicates for each strain), and the bar plots are mean ± S.D. $p$ values are from one-tailed Student's $t$-test.

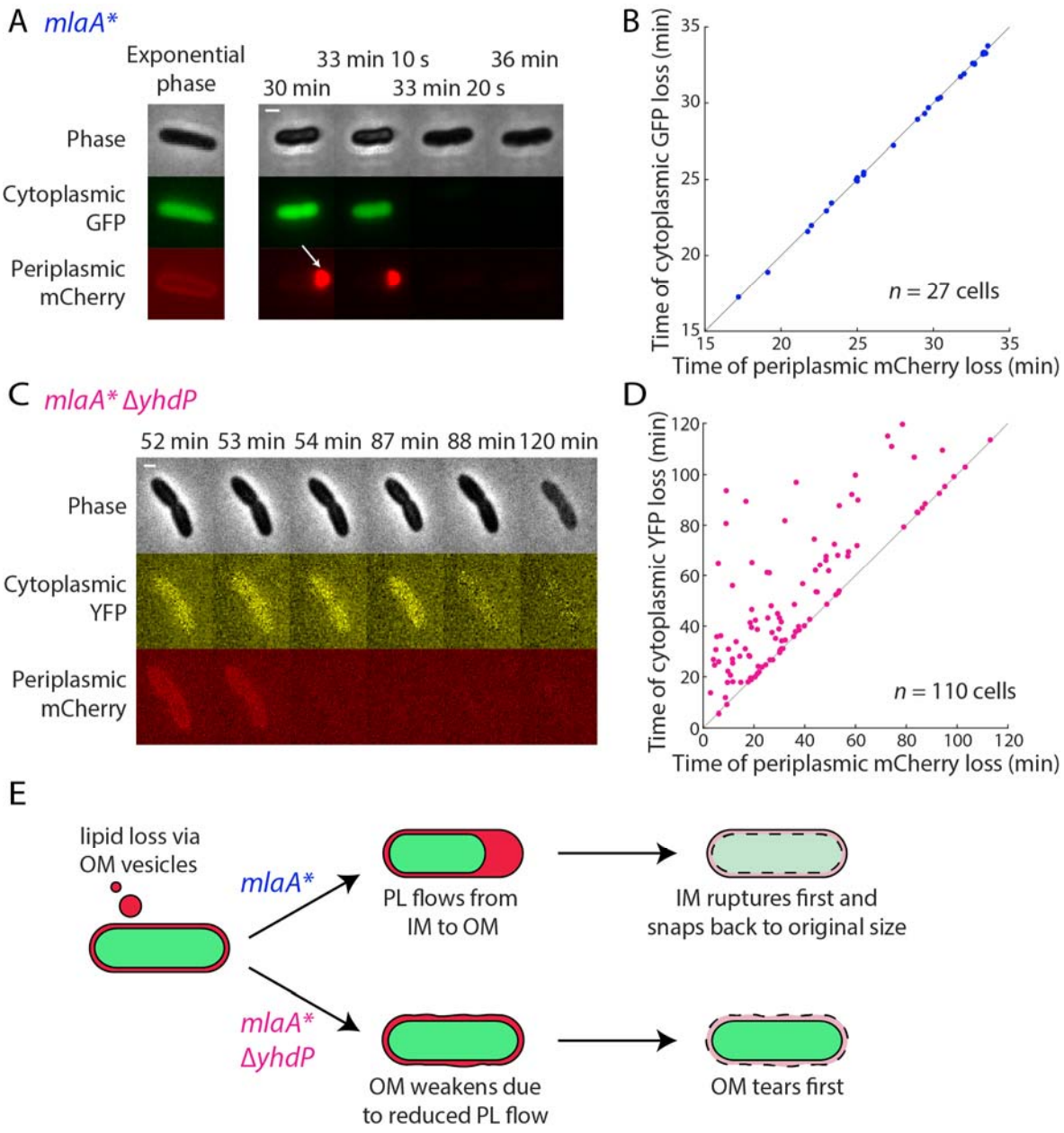


**Figure 5: Deletion of *yhdP* from *mlaA** cells causes the OM to rupture before the IM in spent medium.**

A) Death trajectory of *mlaA** cells on an agarose pad with spent medium. Cells were labelled with periplasmic mCherry and cytoplasmic GFP. During shrinkage, PLs flowed from the IM to the OM, causing the IM to shrink away from the cell wall

and OM. As a result, periplasmic mCherry was enriched at one cell pole (white arrow). At the time of "popping," both fluorescence signals were lost in the same frame. Scale bar is 1 μm.

B) During the transition to spent medium, mCherry and GFP signals were lost simultaneously in all *mlaA** cells ($n$=27). Dots represent single cells, and black line is $x = y$. The dots are slightly jittered to visualize overlapping data.

C) Death trajectory of *mlaA** Δ*yhdP* cells on an agarose pad with spent medium. Cells were labelled with periplasmic mCherry and cytoplasmic YFP. During the period of shrinkage (52-87 min), the IM did not shrink away from cell wall and OM, as shown by the uniform mCherry signal around the cell periphery. The cell also lost its periplasmic mCherry signal tens of minutes before losing cytoplasmic YFP signal, suggesting that the OM ruptured before the IM. Scale bar is 1 μm.

D) During the transition to spent medium, the mCherry signal was lost at least 2 min before the YFP signal in $n$=74 (out of 110) *mlaA** Δ*yhdP* cells, indicating that deletion of *yhdP* leads to rupture of the OM before the IM. In all other cells both signals were lost simultaneously. Dots represent single cells, and black line is $x = y$. The dots are slightly jittered to visualize overlapping data.

E) Model of Δ*yhdP*-mediated death. The *mlaA** mutation leads to membrane loss via OM vesicles and disrupts PL homeostasis during the transition into stationary

557 phase. In the *mlaA** background (top), PLs flow from the IM to the OM to
558 replenish the membrane loss, causing the IM to shrink away from OM, and
559 eventually leading to cell death through IM rupture. By contrast, in *mlaA** Δ*yhdP*
560 cells (bottom), deletion of *yhdP* suppresses PL flow, leading to further weakening
561 of an already compromised OM that ruptures before the IM.
562

# Tables

**Table 1: Percentage of reads in the *mlaA** library mapping to suppressor genes following three successive overnight incubations in spent medium.**

| Gene name | % of total reads, incubation 1 | % of total reads, incubation 2 | % of total reads, incubation 3 |
|---|---|---|---|
| *mlaA* | 48.1 | 84.1 | 86.0 |
| *pldA* | 14.7 | 9.8 | 10.3 |
| *lptC* | 8.6 | 0.9 | 0 |
| *dsbA* | 4.5 | 0 | 0 |
| *yaiP* | 1.3 | 2.7 | 1.7 |
| *acs* | 0.7 | 0 | 0 |
| *fadE* | 0.6 | 0 | 0 |
| *secA* | 0.5 | 0 | 0 |
| *asmA* | 0.3 | 0 | 0 |
| *yejM* | 0.2 | 0 | 0 |

Genomic DNA was extracted from the *mlaA** library following overnight incubation, which induces lysis, and transposon junctions were sequenced. Reads were mapped to the *E. coli* MC4100 genome and open reading frames were quantified to identify which gene disruptions were enriched after each incubation and hence were potential

571 suppressors. The two known strongest suppressors of *mlaA**, *mlaA* and *pldA*, quickly

572 predominated in the culture.

**Table 2: Number of reads in the *mlaA** and Δ*mlaA* libraries mapping to various genes after a two-hour incubation in spent medium.**

| Gene name | # of reads – *mlaA** | # of reads – Δ*mlaA* | $\log_2$(*mlaA**/Δ*mlaA*) |
|---|---|---|---|
| *yhdP* | 2,512,727 | 49,893 | 5.7 |
| *cyaA* | 1,153,018 | 83,061 | 3.8 |
| *mlaA* | 680,035 | N/A | N/A |
| *cysG* | 348,756 | 13,056 | 4.7 |
| *rbsD* | 215,556 | 13,903 | 4.0 |
| *sdhA* | 139,279 | 16,305 | 3.1 |
| *rssB* | 138,738 | 3885 | 5.2 |

Genomic DNA was extracted from the *mlaA** and Δ*mlaA* libraries following 2 h of incubation in spent medium, and transposon junctions were sequenced. Reads were mapped to the *E. coli* MC4100 genome and open reading frames were quantified. The most abundant gene disruption in the *mlaA** library was *yhdP*.

579 **Supplementary Tables**

580

581 **Table S1: Strains used in this study.**

| ***Escherichia coli* K-12 strains** | **Genotype and relevant features** | **Reference** |
|---|---|---|
| MC4100 | F-*araD139 (argF-lac)U169 rpsL150 relA1 flb5301 deoC1 ptsF25 thi* | (35) |
| HC735 | MC4100 ara+ Δ*yfdI* | (10, 36) |
| HC687 | MC4100 ara+ Δ*yfdI mlaA** | (10, 27) |
| HC736 | MC4100 ara+ Δ*yfdI* Δ*mlaA* | (10, 27, 37) |
| JG153 | MC4100 ara+ Δ*yfdI* Δ*yhdP::kan* | (10, 27) and this study |
| JG152 | MC4100 ara+ Δ*yfdI mlaA** Δ*yhdP::kan* | (10, 27) and this study |
| JG174 | MC4100 ara+ Δ*yfdI intS::tn10* | This study |
| JG178 | MC4100 ara+ Δ*yfdI mlaA** *intS::tn10* | This study |

| | | |
|---|---|---|
| JG176 | MC4100 ara+ Δ*yfdI mlaA** *intS::tn10* Δ*yhdP* | (27, 37) and this study |
| JG179 | MC4100 ara+ Δ*yfdI mlaA** *intS::tn10* Δ*yhdP* Δ*wzzE::kan* | (27, 37) and this study |
| JG197 | MC4100 ara+ Δ*yfdI mlaA** *intS::tn10* Δ*wzzE::kan* | (27, 37) and this study |
| KC637 | HC687 pMT37-*sulA* | (10) |
| KC626 | HC687 attHK:*Plac-mCherry* pZS21-*GFP* | (10) |
| KC1307 | JG153 attHK:*Plac-mCherry* *Plac-YFP* | (10) and this study |

582

583 **References**


584 1. H. Nikaido, Outer membrane of *Salmonella typhimurium*: transmembrane
585 diffusion of some hydrophobic substances. *BBA-Biomembranes* **433**, 118-132
586 (1976).

587 2. H. Nikaido, Molecular basis of bacterial outer membrane permeability revisited.
588 *Microbiol. Mol. Biol. Rev.* **67**, 593-656 (2003).

589 3. A. Kovacs-Simon, R. Titball, S. L. Michell, Lipoproteins of bacterial pathogens.
590 *Infect. Immun.* **79**, 548-561 (2011).

591 4. S. Okuda, E. Freinkman, D. Kahne, Cytoplasmic ATP hydrolysis powers
592 transport of lipopolysaccharide across the periplasm in *E. coli*. *Science* **338**, 1214-
593 1217 (2012).

594 5. S. Okuda, D. J. Sherman, T. J. Silhavy, N. Ruiz, D. Kahne, Lipopolysaccharide
595 transport and assembly at the outer membrane: The PEZ model. *Nat. Rev.*
596 *Microbiol.* **14**, 337-349 (2016).

597 6. A. Konovalova, T. J. Silhavy, Outer membrane lipoprotein biogenesis: Lol is not
598 the end. *Philos. T. R. Soc. B* **370**, 20150030 (2015).

599 7. N. W. Rigel, T. J. Silhavy, Making a beta-barrel: Assembly of outer membrane
600 proteins in Gram-negative bacteria. *Curr. Opin. Microbiol.* **15**, 189-193 (2012).

601 8. N. C. Jones, M. J. Osborn, Translocation of phospholipids between the outer and
602 inner membranes of *Salmonella typhimurium*. *J. Biol. Chem.* **252**, 7405-7412 (1977).

9. J. C. Malinverni, T. J. Silhavy, An ABC transport system that maintains lipid asymmetry in the Gram-negative outer membrane. *Proc. Natl. Acad. Sci. U.S.A.* **106**, 8009-8014 (2009).

10. H. A. Sutterlin *et al.*, Disruption of lipid homeostasis in the Gram-negative cell envelope activates a novel cell death pathway. *Proc. Natl. Acad. Sci. U.S.A.* **113**, E1565-E1574 (2016).

11. J. Abellón-Ruiz *et al.*, Structural basis for maintenance of bacterial outer membrane lipid asymmetry. *Nat. Microbiol.* **2**, 1616-1623 (2017).

12. K. L. May, T. J. Silhavy, The *Escherichia coli* phospholipase PldA regulates outer membrane homeostasis via lipid signaling. *mBio* **9** (2018).

13. A. M. Mitchell, W. Wang, T. J. Silhavy, Novel RpoS-dependent mechanisms strengthen the envelope permeability barrier during stationary phase. *J. Bacteriol.* **199** (2017).

14. E. Bi, J. Lutkenhaus, Cell division inhibitors SulA and MinCD prevent formation of the FtsZ ring. *J. Bacteriol.* **175**, 1118-1125 (1993).

15. A. M. Mitchell, T. Srikumar, T. J. Silhavy, Cyclic enterobacterial common antigen maintains the outer membrane permeability barrier of *Escherichia coli* in a manner controlled by YhdP. *mBio* **9** (2018).

16. E. R. Rojas *et al.*, The outer membrane is an essential load-bearing element in Gram-negative bacteria. *Nature* **559**, 617-621 (2018).

17. L. Leive, V. K. Shovlin, S. E. Mergenhagen, Physical, chemical, and immunological properties of lipopolysaccharide released from *Escherichia coli* by ethylenediaminetetraacetate. *J. Biol. Chem.* **243**, 6384-6391 (1968).

18. N. A. Amro *et al.*, High-resolution atomic force microscopy studies of the *Escherichia coli* outer membrane: structural basis for permeability. *Langmuir* **16**, 2789-2796 (2000).

19. M. Bayer, Areas of adhesion between wall and membrane of *Escherichia coli*. *Microbiology* **53**, 395-404 (1968).

20. E. Kellenberger, The 'Bayer bridges' confronted with results from improved electron microscopy methods. *Mol. Microbiol.* **4**, 697-705 (1990).

21. N. C. Jones, M. J. Osborn, Interaction of *Salmonella typhimurium* with phospholipid vesicles. Incorporation of exogenous lipids into intact cells. *J. Biol. Chem.* **252**, 7398-7404 (1977).

22. T. P. Levine, Remote homology searches identify bacterial homologues of eukaryotic lipid transfer proteins, including Chorein-N domains in TamB and AsmA and Mdm31p. *BMC Mol Cell Biol* **20**, 43 (2019).

23. N. Kumar *et al.*, VPS13A and VPS13C are lipid transport proteins differentially localized at ER contact sites. *J. Cell Biol.* **217**, 3625-3639 (2018).

641 24. P. Li, J. A. Lees, C. P. Lusk, K. M. Reinisch, Cryo-EM reconstruction of a VPS13
642 fragment reveals a long groove to channel lipids between membranes. *J. Cell Biol.*
643 **219** (2020).
644 25. I. Josts *et al.*, The Structure of a Conserved Domain of TamB Reveals a
645 Hydrophobic β Taco Fold. *Structure* **25**, 1898-1906 (2017).
646 26. J. A. Lees, K. M. Reinisch, Inter-organelle lipid transfer: a channel model for
647 Vps13 and chorein-N motif proteins. *Curr. Opin. Cell Biol.* **65**, 66-71 (2020).
648 27. T. Baba *et al.*, Construction of *Escherichia coli* K-12 in-frame, single-gene knockout
649 mutants: The Keio collection. *Mol. Syst. Biol.* **2**, 2006-0008 (2006).
650 28. T. J. Silhavy, M. L. Berman, L. W. Enquist, *Experiments with gene fusions* (Cold
651 Spring Harbor Laboratory, 1984).
652 29. K. A. Datsenko, B. L. Wanner, One-step inactivation of chromosomal genes in
653 *Escherichia coli* K-12 using PCR products. *Proc. Natl. Acad. Sci. U.S.A.* **97**, 6640-
654 6645 (2000).
655 30. G. C. Langridge *et al.*, Simultaneous assay of every *Salmonella Typhi* gene using
656 one million transposon mutants. *Genome Res.* **19**, 2308-2316 (2009).
657 31. A. Edelstein, N. Amodaj, K. Hoover, R. Vale, N. Stuurman, Computer control of
658 microscopes using μManager. *Curr. Protoc. Mol. Biol.* **92**, 14-20 (2010).
659 32. D. A. Van Valen *et al.*, Deep learning automates the quantitative analysis of
660 individual cells in live-cell imaging experiments. *PLoS Comp. Biol.* **12** (2016).

661 33. T. Ursell *et al.*, Rapid, precise quantification of bacterial cellular dimensions
662 across a genomic-scale knockout library. *BMC Biol.* **15**, 17 (2017).
663 34. O. Sliusarenko, J. Heinritz, T. Emonet, C. Jacobs-Wagner, High-throughput,
664 subpixel precision analysis of bacterial morphogenesis and intracellular spatio-
665 temporal dynamics. *Mol. Microbiol.* **80**, 612-627 (2011).
666 35. M. J. Casadaban, Transposition and fusion of the *lac* genes to selected promoters
667 in *Escherichia coli* using bacteriophage lambda and Mu. *J. Mol. Biol.* **104**, 541-555
668 (1976).
669 36. N. Ruiz, L. S. Gronenberg, D. Kahne, T. J. Silhavy, Identification of two inner-
670 membrane proteins required for the transport of lipopolysaccharide to the outer
671 membrane of *Escherichia coli*. *Proc. Natl. Acad. Sci. U.S.A.* **105**, 5537-5542 (2008).
672 37. P. P. Cherepanov, W. Wackernagel, Gene disruption in *Escherichia coli*: TcR and
673 KmR cassettes with the option of Flp-catalyzed excision of the antibiotic-
674 resistance determinant. *Gene* **158**, 9-14 (1995).

675

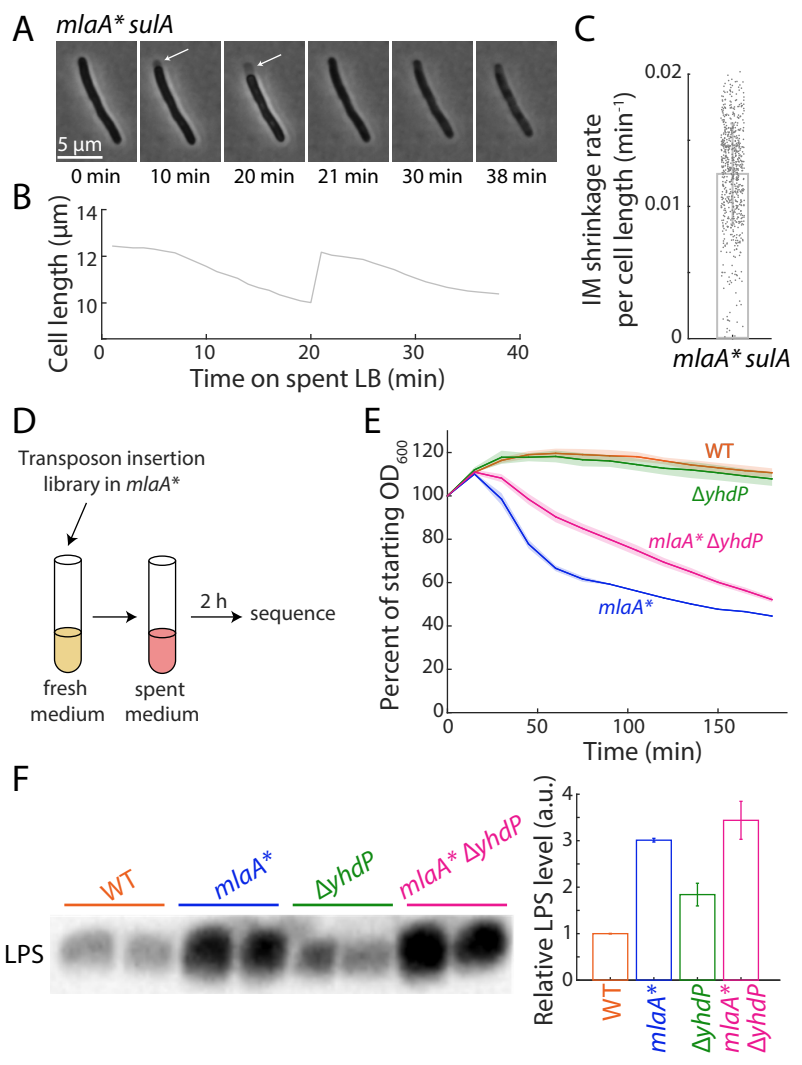
A
mlaA* sulA
5 μm
0 min
10 min
20 min
21 min
30 min
38 min
B
Cell length (μm)
Time on spent LB (min)
C
IM shrinkage rate per cell length (min-1)
mlaA* sulA
D
Transposon insertion library in mlaA*
2 h
sequence
fresh medium
spent medium
E
Percent of starting OD600
Time (min)
WT
ΔyhdP
mlaA* ΔyhdP
mlaA*
F
WT
mlaA*
ΔyhdP
mlaA* ΔyhdP
LPS
Relative LPS level (a.u.)

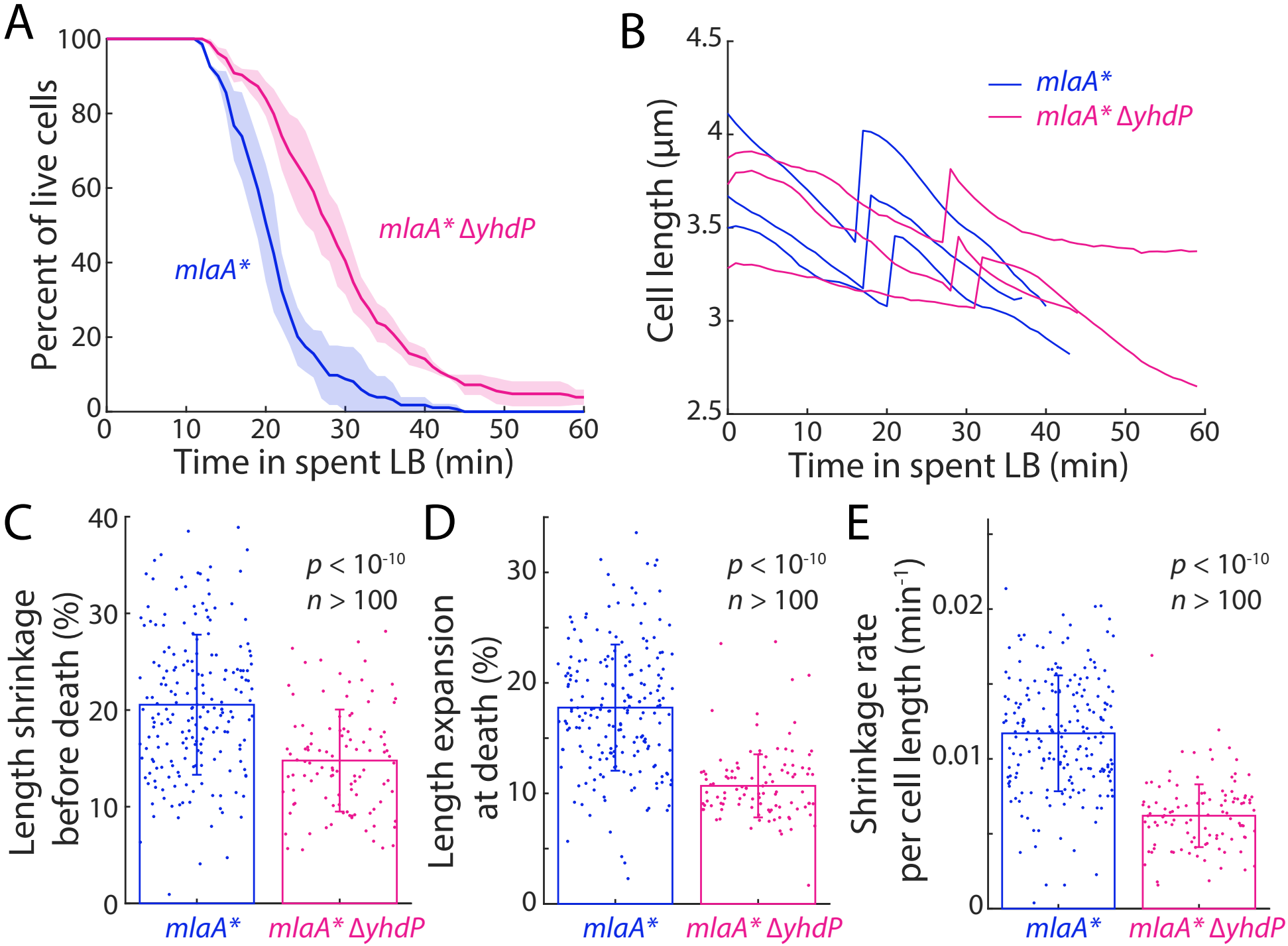
A
Percent of live cells
Time in spent LB (min)
mlaA*
mlaA* ΔyhdP
B
Cell length (μm)
Time in spent LB (min)
mlaA*
mlaA* ΔyhdP
C
Length shrinkage before death (%)
p < 10-10
n > 100
mlaA*
mlaA* ΔyhdP
D
Length expansion at death (%)
p < 10-10
n > 100
mlaA*
mlaA* ΔyhdP
E
Shrinkage rate per cell length (min-1)
p < 10-10
n > 100
mlaA*
mlaA* ΔyhdP

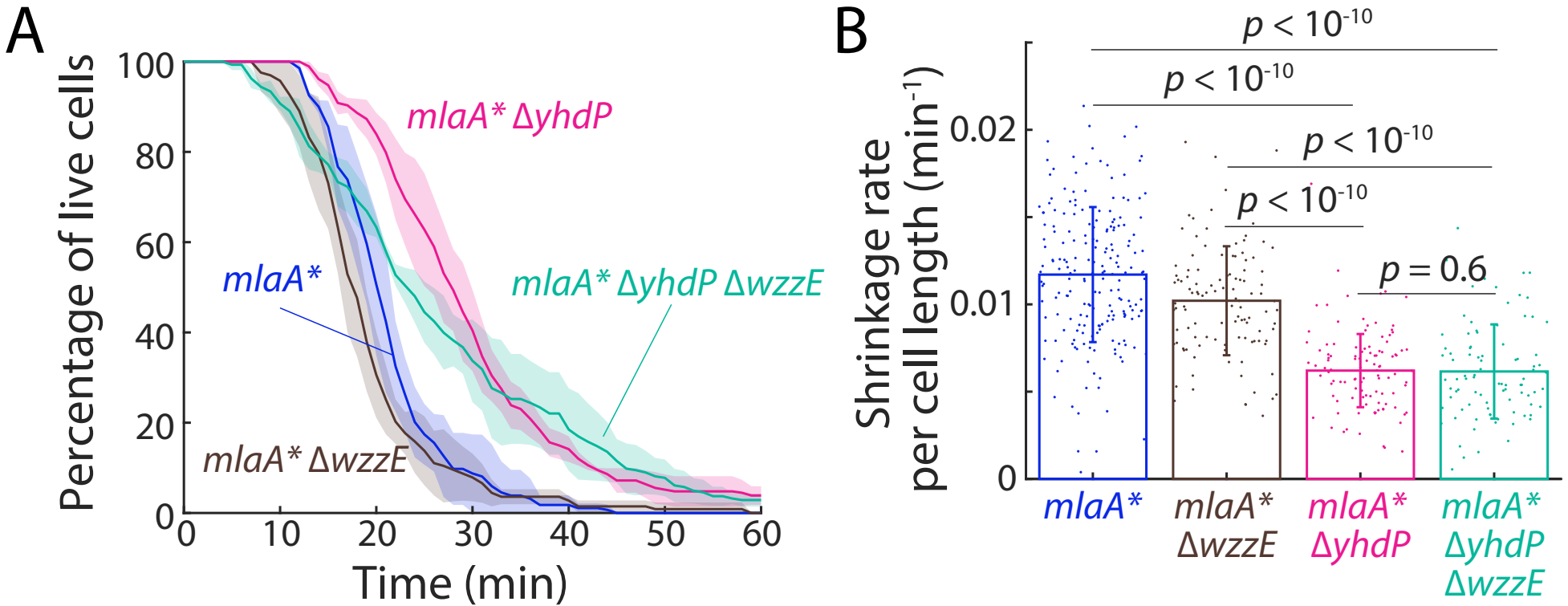
A
Percentage of live cells
100
80
60
40
20
0
0
10
20
30
40
50
60
Time (min)
mlaA* ΔyhdP
mlaA*
mlaA* ΔyhdP ΔwzzE
mlaA* ΔwzzE
B
Shrinkage rate per cell length (min-1)
0.02
0.01
0
p < 10-10
p < 10-10
p < 10-10
p < 10-10
p = 0.6
mlaA*
mlaA* ΔwzzE
mlaA* ΔyhdP
mlaA* ΔyhdP ΔwzzE

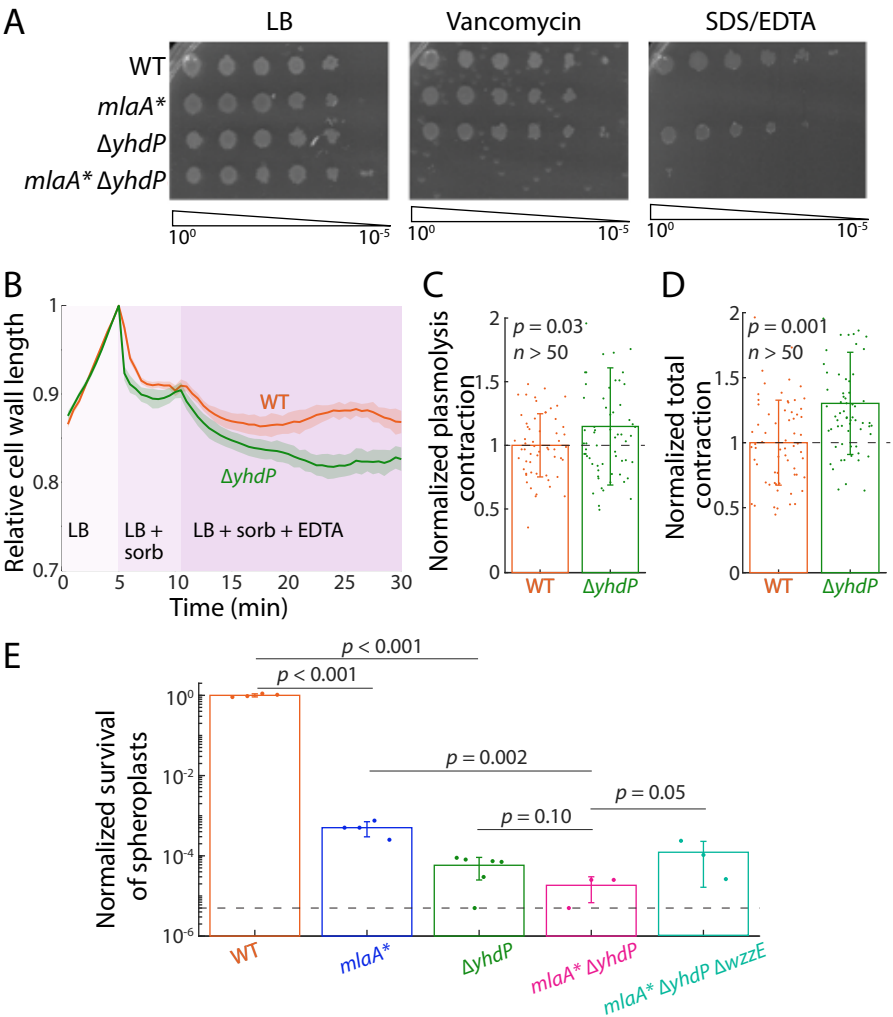
A
LB
Vancomycin
SDS/EDTA
WT
mlaA*
ΔyhdP
mlaA* ΔyhdP
10^0
10^-5
B
Relative cell wall length
WT
ΔyhdP
LB
LB + sorb
LB + sorb + EDTA
Time (min)
C
Normalized plasmolysis contraction
p = 0.03
n > 50
WT
ΔyhdP
D
Normalized total contraction
p = 0.001
n > 50
WT
ΔyhdP
E
Normalized survival of spheroplasts
p < 0.001
p < 0.001
p = 0.002
p = 0.10
p = 0.05
WT
mlaA*
ΔyhdP
mlaA* ΔyhdP
mlaA* ΔyhdP ΔwzzE

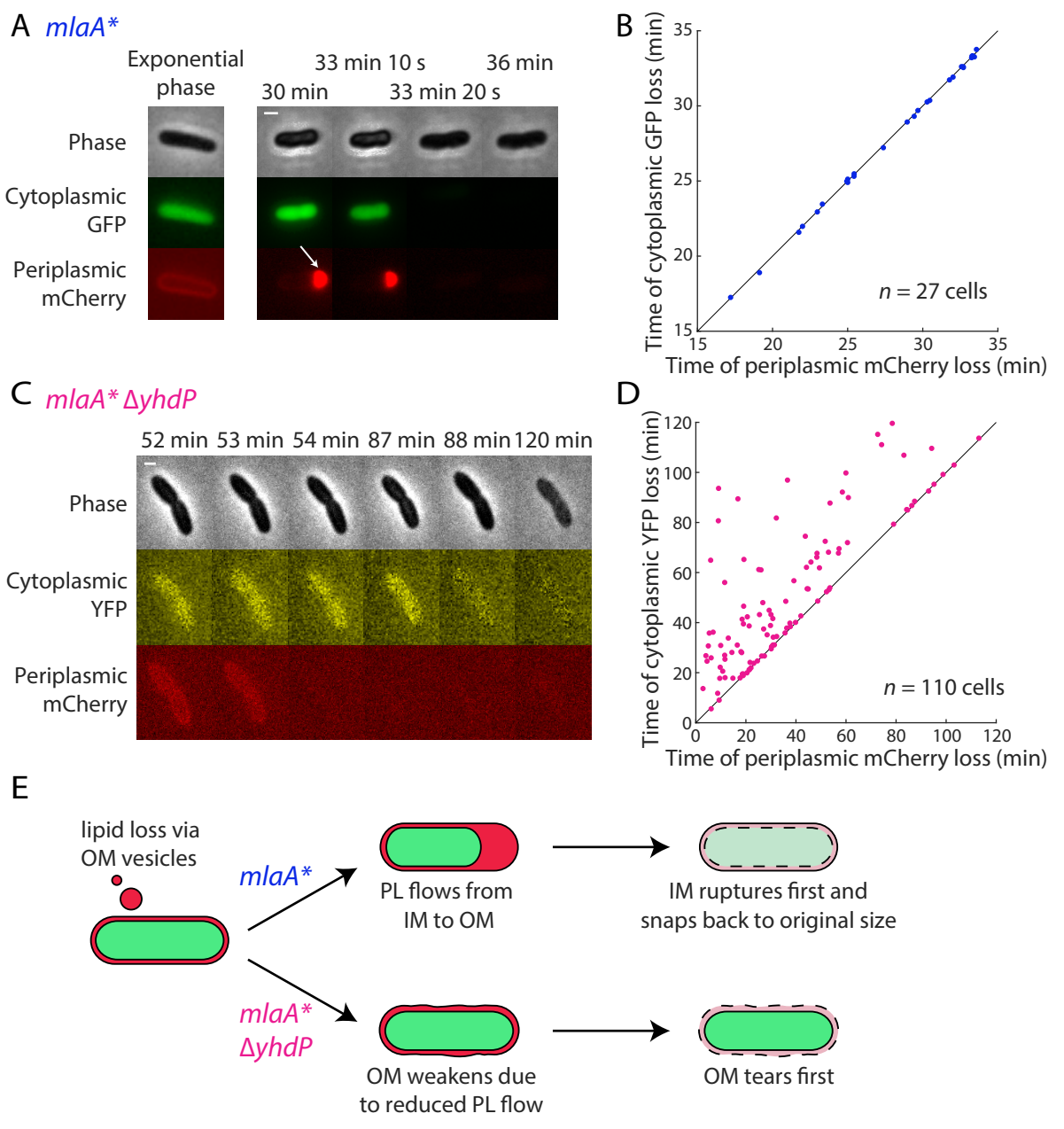
A mlaA*
Exponential phase
30 min
33 min 10 s
33 min 20 s
36 min
Phase
Cytoplasmic GFP
Periplasmic mCherry
B
Time of cytoplasmic GFP loss (min)
Time of periplasmic mCherry loss (min)
n = 27 cells
C mlaA* ΔyhdP
52 min
53 min
54 min
87 min
88 min
120 min
Phase
Cytoplasmic YFP
Periplasmic mCherry
D
Time of cytoplasmic YFP loss (min)
Time of periplasmic mCherry loss (min)
n = 110 cells
E
lipid loss via OM vesicles
mlaA*
PL flows from IM to OM
IM ruptures first and snaps back to original size
mlaA* ΔyhdP
OM weakens due to reduced PL flow
OM tears first